^{139}La NMR investigation of the interplay between lattice, charge, and spin dynamics in the charge-ordered high-T_c cuprate $La_{1.875}Ba_{0.125}CuO_4$

P. M. Singer,[1] A. Arsenault,[2] T. Imai,[2] and M. Fujita[3]

[1]*Department of Chemical and Biomolecular Engineering, Rice University, 6100 Main St., Houston, Texas 77005-1892, USA*

[2]*Department of Physics and Astronomy, McMaster University, Hamilton, Ontario, Canada L8S 4M1*

[3]*Institute for Materials Research, Tohoku University, Sendai 980-8577, Japan*

(Received 1 January 2020; revised manuscript received 3 April 2020; accepted 6 April 2020; published 11 May 2020)

We investigate the interplay between the lattice, charge, and spin dynamics in charge-ordered high T_c cuprate $La_{1.875}Ba_{0.125}CuO_4$ ($T_c = 4$ K) based on the inverse Laplace transform (ILT) analysis of the ^{139}La nuclear spin-lattice relaxation rate $1/T_1$ (dubbed ILTT$_1$ analysis hereafter). A major thrust of the ILTT$_1$ analysis is that one can deduce the probability density function $P(1/T_1)$ of distributed $1/T_1$. We demonstrate that $1/T_1^{\rm lm}$, defined as the log mean (i.e., the center of gravity on a logarithmic scale) of $P(1/T_1)$, can be well approximated by $1/T_1^{\rm str}$ deduced from the phenomenological stretched fit; however, $P(1/T_1)$ can provide much richer insight into how the lattice, charge, and spin fluctuations and their distribution develop near and below the long-range charge order at $T_{\rm charge} \sim 54$ K. Upon entering the charge-ordered state, a divergent increase of $1/T_1^{\rm lm}$ toward the spin ordering at $T_{\rm spin}^{\mu\rm SR} \simeq 35$ K is accompanied by an asymmetric broadening of $P(1/T_1)$. Even deep inside the charge-ordered state, $1/T_1$ at a gradually diminishing fraction of ^{139}La sites continues to slow down as temperature is lowered, as expected for canonical superconducting CuO_2 planes without enhanced spin fluctuations. The fraction of such canonical ^{139}La sites almost disappears by $\simeq 40$ K. In contrast, nearly half of the ^{139}La sites in $La_{1.885}Sr_{0.115}CuO_4$ ($T_{\rm charge} \simeq 80$ K) still exhibit the canonical behavior without enhanced spin fluctuations even near its $T_c = 31$ K. These contrasting behaviors explain why superconductivity in $La_{1.875}Ba_{0.125}CuO_4$ is more strongly suppressed than in $La_{1.885}Sr_{0.115}CuO_4$ despite the lower onset temperature of the charge order.

DOI: 10.1103/PhysRevB.101.174508

I. GENERAL INTRODUCTION

In $La_{2-x}Sr_xCuO_4$, the high-temperature superconducting phase with the critical temperature as high as $T_c = 38$ K manifests itself after the high-temperature tetragonal (HTT) to low-temperature orthorhombic (LTO) structural phase transition takes place around $\simeq 200$ K. In contrast, $La_{2-x}Ba_xCuO_4$ undergoes an additional structural phase transition from the LTO to the low-temperature tetragonal (LTT) phase below $T_{\rm LTO\text{-}LTT} \simeq 60$ K, and T_c in the LTT structure is anomalously suppressed to as low as $T_c \simeq 4$ K near the magic composition with $x \simeq 1/8$ [1]. μSR measurements uncovered the presence of spin order below $T_{\rm spin}^{\mu\rm SR} \simeq 35$ K in $La_{1.875}Ba_{0.125}CuO_4$ [2].

Nd codoping into $La_{2-x}Sr_xCuO_4$ also induces the same sequence of structural transitions from HTT to LTO, and then to LTT. It was in $La_{1.48}Nd_{0.4}Sr_{0.12}CuO_4$ where Tranquada *et al.* [3] discovered the charge-order transition at $T_{\rm charge} \simeq 60$ K in the LTT phase based on neutron diffraction measurements. Subsequent NMR [4,5] and neutron scattering experiments [6] showed that a charge-order transition also accompanies the LTO to LTT structural transition in $La_{1.875}Ba_{0.125}CuO_4$. More recently, x-ray scattering experiments [7,8] revealed the presence of dynamic short-range charge order in $La_{1.875}Ba_{0.125}CuO_4$ prior to the onset of long-range charge order at $T_{\rm charge} \simeq 54$ K [8].

There has been a long history in the NMR investigation of the complicated behavior of $La_{2-x}Ba_xCuO_4$ [4,5,9–15], yet our understanding of the interplay between the lattice, charge, and spin degrees of freedom near charge order is still far from complete. This is in part because the NMR spin-lattice relaxation rate $1/T_1$ develops a large distribution near and below $T_{\rm charge}$, and the NMR community in condensed-matter physics did not have the machinery to accurately probe the nature and extent of the distribution. Furthermore, the phenomenological approach to deduce $1/T_1$ based on the stretched exponential fit of the nuclear spin recovery curve $M(t)$ cannot distinguish the fluctuations of the electric field gradient (EFG) and spins.

In this paper, we shed light on the complex behavior of $La_{1.875}Ba_{0.125}CuO_4$ by analyzing the $1/T_1$ recovery curve $M(t)$ observed at the ^{139}La sites based on the inverse Laplace transform (ILT) analysis techniques (dubbed ILTT$_1$ analysis hereafter). The ILT in the context of NMR has been conceptually known for some time [16], and applied successfully in petrophysics [17–21] and condensed-matter physics [22,23] by numerically inverting $M(t)$. A major thrust of the ILTT$_1$ analysis is that *one can generate the histogram of distributed* $1/T_1$ *without presuming any particular functional form of the density function* $P(1/T_1)$, in addition to the log mean $1/T_1^{\rm lm}$ (i.e., the center of gravity on a logarithmic scale) of the distributed relaxation rate. We will demonstrate that slow lattice and/or charge fluctuations develop at the NMR frequency scales below $\simeq 80$ K, where the dynamic short-range charge order develops [8]. Comparison of $P(1/T_1)$ between $La_{1.875}Ba_{0.125}CuO_4$ ($T_c = 4$ K) and $La_{1.885}Sr_{0.115}CuO_4$

($T_c \simeq 31$ K) also reveals a qualitative difference between the two. The volume fraction of the canonically superconducting domains in the CuO_2 planes without enhanced spin fluctuations is reduced to almost null in $La_{1.875}Ba_{0.125}CuO_4$ below $\simeq 40$ K, whereas nearly half of the volume still behaves as a canonical superconductor in $La_{1.885}Sr_{0.115}CuO_4$.

The rest of this paper is organized as follows. In Sec. II, we explain the key aspects of the ILT techniques and what the $ILTT_1$ analysis can (not) do. Section III outlines the experimental methods, and Sec. IV discusses the results, followed by summary and conclusions in Sec. V.

II. INVERSE LAPLACE TRANSFORM OF $M(t)$

To measure the spin-lattice relaxation time T_1, one applies an inversion pulse and monitors the recovery curve $M(t)$ of the nuclear magnetization as a function of time t. In the simplest case of nuclear spin $I = 1/2$ with a single, nondistributed value of $1/T_1$, the recovery obeys an exponential form as such,

$$M(t) = M_0 - A\, e^{-t/T_1}, \tag{1}$$

where M_0 is the saturated value of the nuclear magnetization and A ($\leqslant 2M_0$) represents the degree of inversion.

Magnetic inhomogeneity of the sample results in a distribution of $1/T_1$, and $M(t)$ may exhibit a stretched exponential form under certain circumstances [16,24,25],

$$M(t) = M_0 - A\, e^{-\left(t/T_1^{\rm str}\right)^{\beta}}, \tag{2}$$

where β is the stretched exponent less than 1. If $1/T_1$ has no distribution, $1/T_1^{\rm str} = 1/T_1$ and $\beta = 1$. For example, in the case of $1/T_1$ measured by ^{63}Cu nuclear quadrupole resonance (NQR) techniques in a highly disordered $YBa_2Cu_3O_{6.9}$ sample ($T_c = 92$ K), Eq. (2) worked well far below T_c with the exponent $\beta = 1/2$ [26], which is expected for diffusionless, enhanced relaxation caused by defect spins [24,25]. One can justify such a stretched fit, if $\ln[M_0 - M(t)]$ versus t^{β} or $\ln[M_0 - M(t)]$ versus $\ln(t)$ yields a straight line [24,26].

One needs to bear in mind that the distributed relaxation mechanisms do not always lead to the stretched form in Eq. (2). In fact, Eq. (2) failed for $YBa_2Cu_3O_{6.95}$ ($T_c = 92$ K) with less magnetic defects [27,28]. Instead, a two-component fit worked well, with two distinct values of fast and slow relaxation rates, $1/T_1^{\rm fast}$ and $1/T_1^{\rm slow}$:

$$M(t) = M_0 - A_{\rm fast} e^{-t/T_1^{\rm fast}} - A_{\rm slow} e^{-t/T_1^{\rm slow}}. \tag{3}$$

In this case, dilute defect spins affect only the nuclear spins in their vicinity, and the rest of the superconductor exhibits much longer, intrinsic $1/T_1^{\rm slow}$. An analogous situation arises for $1/T_1$ measured for type-II superconductors under the presence of vortex cores induced by an external magnetic field. Accordingly, in NMR research on superconductivity, it is usually $1/T_1^{\rm slow}$ that researchers present far below T_c.

A dilemma arises if there is no clear-cut justification for Eq. (2) or (3). In fact, in the case of ^{19}F ($I = 1/2$) NMR investigations of the diluted antiferromagnet $Mn_{1-x}Zn_xF_2$, the $\ln[M_0 - M(t)]$ versus $\ln(t)$ plot revealed that the experimental reality is the combination of Eqs. (2) and (3) [24]. Furthermore, additional complications arise if $M(t)$ under consideration is not for $I = 1/2$. For example, ^{139}La is a spin $I = 7/2$ nucleus. In an ideal case of nondistributed $1/T_1$, $M(t)$ for the $I_z = -1/2 \leftrightarrow +1/2$ (i.e., central) transition of $I = 7/2$ can be written analytically as a linear combination of four normal modes [29,30],

$$M(t) = M_0 - A \sum_{k=1}^{4} p_k e^{-q_k t/T_1}, \tag{4}$$

where p_k={1/84, 3/44, 75/364, 1225/1716} and q_k={1, 6, 15, 28}, and $\sum_{k=1}^{4} p_k = 1$ is normalized. In this case, the aforementioned log plot $\ln[M_0 - M(t)]$ does not yield a straight line, even if there is no distribution in $1/T_1$. Then how should we choose and justify the appropriate fitting function for $M(t)$ when $1/T_1$ is distributed and the fit with Eq. (4) is unsatisfactory? Should we just stretch each exponential term as in Eq. (2) or consider two or more values of $1/T_1$ as in Eq. (3)? Or a combination of both?

The $ILTT_1$ analysis technique tells us the answers to these questions. Regardless of the origin of the distribution of $1/T_1$ and its extent, one can actually *deduce* the probability density function $P(1/T_1)$ of $1/T_1$ based on the ILT of $M(t)$ [21]. The ILT consists of fitting $M(t)$ to a sum of exponentials with decay rate $1/T_{1j}$ and weight $P(1/T_{1j}) \geqslant 0$. For the simplest case of $I = 1/2$, the discrete form of the ILT inverts for $P(1/T_1)$, assuming the following expression for the experimental data $M(t)$ [17–21]:

$$M(t) = \sum_{j=1}^{m} \left[1 - 2\, e^{-t/T_{1j}}\right] P(1/T_{1j}). \tag{5}$$

For simplicity, we assumed perfect inversion (i.e., $A = 2M_o$). The summation $\sum_{j=1}^{m} P(1/T_{1j}) = M_0$ is the saturated value of the magnetization and $m = 250$ is the chosen number of logarithmically spaced bins in the $P(1/T_1)$ distribution. The normalization used to convert $P(1/T_1)$ into a probability density is detailed in Sec. IV B. See the Supplemental Material [31] as well as Refs. [17–21,32–34] for the method to deal with the imperfect inversion in actual experimental data, the details of the mathematical background, and the general procedures for the ILT. Note that, technically, Eq. (5) is the discrete form of a Fredholm integral equation of the first kind [35], but for simplicity we refer to it here as an ILT.

The advantage of ILT is that we need not assume phenomenological functional forms for $M(t)$, such as Eq. (2) or (3). The only assumption in the ILT is that $M(t)$ decays as a sum of exponentials with decay rates $1/T_{1j}$, implying a heterogeneous distribution in $1/T_1$ over the sample. If the distribution of $1/T_1$ is peaked at one value, $P(1/T_1)$ deduced from $M(t)$ will have one peak (i.e., be a delta function if $1/T_1$ has no distribution) at the most likely value of $1/T_1$. On the other hand, if $1/T_1$ is distributed around two distinctive values, as is the case for Eq. (3), $P(1/T_1)$ will have two peaks centered at $1/T_1^{\rm fast}$ and $1/T_1^{\rm slow}$.

It is useful to show how $ILTT_1$ analysis works based on a simple example. In Fig. 1(a), we generated a model relaxation curve $M(t)$ consisting of discrete data points represented by black dots. The best fit of the model data with Eq. (2) (red curve) yields $1/T_1^{\rm str} = 1.44\ {\rm s}^{-1}$ and $\beta = 0.89$. The fit seems very good, and the deviation from $\beta = 1$ is fairly small. Accordingly, one would be tempted to conclude that $P(1/T_1)$

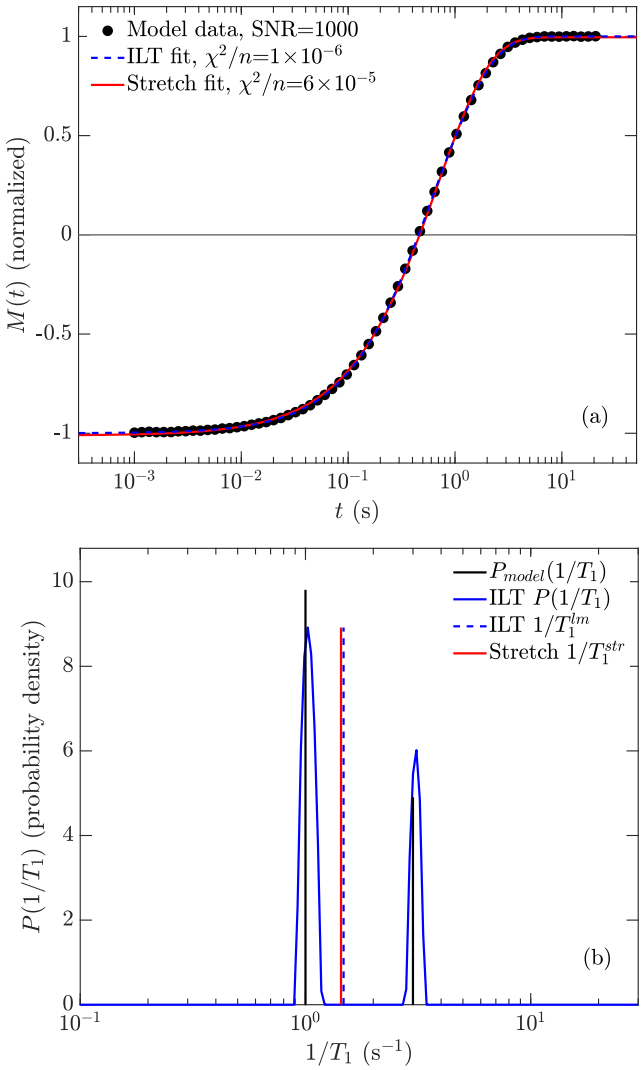

FIG. 1. (a) Model data $M(t)$ (•), normalized by $M(t)/M_0$, generated for demonstration purposes using Eq. (6) as described in the main text, with $n = 64$ log-spaced data points. Solid red curve is the best stretched single exponential fit with Eq. (2) with $1/T_1^{\rm str} = 1.44\,{\rm s}^{-1}$ and $\beta = 0.89$, under the false assumption that there is only one peak in $P(1/T_1)$ centered around $1/T_1^{\rm str}$. Dashed blue curve is the best ILT fit with Eq. (5) resulting in $P(1/T_1)$, represented by the blue curve in panel (b). Note how the ILT fit yields a lower mismatch χ^2/n than the stretched exponential fit. (b) Black vertical lines represent $P_{\rm model}(1/T_1)$ from Eq. (6), consisting of two delta functions at $1/T_1^{\rm fast}$ and $1/T_1^{\rm slow}$. Blue curve represents the ILT spectrum $P(1/T_1)$ (probability density) of the $M(t)$ data points in (a). Notice that $1/T_1^{\rm str}$ (red vertical line) is a good approximation of the log mean $1/T_1^{\rm lm}$ (dashed blue vertical line) of $P(1/T_1)$; however, the stretched fit misses all of the detail in the underlying model $P(1/T_1)_{\rm model}$.

is narrow and peaked around 1.5 s^{-1}, and hence may be close to a delta function as represented by the red vertical line in Fig. 1(b).

However, in reality, we generated the discrete $M(t)$ data in Fig. 1(a) using a two-component function as such:

$$M(t) = 1 - 2/3\,e^{-3t} - 4/3\,e^{-t}. \qquad (6)$$

This is similar to the model in Eq. (3), with $1/T_1^{\rm fast} = 3\,{\rm s}^{-1}$, $1/T_1^{\rm slow} = 1\,{\rm s}^{-1}$, $M_o = 1$, $A_{\rm fast} = 2/3$, and $A_{\rm slow} = 4/3$, plus random noise at the level of 0.1% (i.e., a signal to noise ratio of SNR = 1000). The ILT of the model data in Fig. 1(a) results in $P(1/T_1)$ with double peaks at $1/T_1^{\rm fast}$ and $1/T_1^{\rm slow}$, as shown by a blue curve in Fig. 1(b). The log mean (i.e., center of gravity on a log scale) of $P(1/T_1)$ is located at $1/T_1^{\rm lm} = 1.48\,{\rm s}^{-1}$ (represented by a dashed blue line). The finite width of the blue curve originates from the discreteness of the model data and the built-in random noise [31].

This simple example illustrates the power of ILT and the potentially risky nature of the commonly used stretched exponential fit. While $1/T_1^{\rm str}$ is indeed close to the real log mean $1/T_1^{\rm lm}$ of $P(1/T_1)$, the imagined distribution spectrum shown by a single vertical red line in Fig. 1(b) does not even remotely resemble the true, double peak structure in $P(1/T_1)$.

III. EXPERIMENTAL

We grew a single-crystal sample of $La_{1.875}Ba_{0.125}CuO_4$ ($T_c = 4$ K) based on the traveling solvent floating zone technique at Tohoku [6]. We aligned and cut a small piece of single crystal with the total mass of 51 mg for this study. We conducted ^{139}La NMR measurements at 9 T applied along the c axis with the standard $\pi/2 - \pi$ spin-echo pulse sequence. The ^{139}La NMR line shapes observed for the nuclear spin $I_z = +1/2 \leftrightarrow -1/2$ central transition were very similar to an earlier report [36].

We note that $La_{1.875}Ba_{0.125}CuO_4$ showed a partial loss of ^{139}La signal (i.e., partial ^{139}La wipeout) in the vicinity of ∼35 K, where the signal dropped to ∼1/3 of the full intensity. As such, the ILT may underestimate the distribution in fast $1/T_1$ components in the vicinity of ∼35 K. This is similar to previous reports of ^{139}La wipeout in $La_{1.8-x}Eu_{0.2}Sr_xCuO_4$ (see Fig. 16 in Ref. [5]), but will not affect our conclusions. By contrast, $La_{1.885}Sr_{0.115}CuO_4$ showed no signs of ^{139}La wipeout for $T > T_c$ [22].

We measured $1/T_1$ using the inversion recovery method by applying a π pulse prior to the spin-echo sequence. We summarize the representative results of $M(t)$ in Fig. 2. Measurements of $1/T_1^{\rm str}$ with reasonable accuracy is an easy task and can usually be completed in less than 1 hour at each temperature. However, the accuracy of $M(t)$ required for ILT is far less forgiving, because the resolution of the ILT curve $P(1/T_1)$ can depend on the experimental noise (i.e., the signal-to-noise ratio) of the $M(t)$ curve [31]. In addition, we had to use long spin-echo recycling time up to 240 s between the spin-echo sequences, so we can properly capture the longest components of $1/T_1$ in $M(t)$. For these reasons, it took up to 24 hours to measure $M(t)$ at a given temperature.

IV. ^{139}La NMR RESULTS AND DISCUSSIONS

A. Conventional stretched fit results $1/T_1^{\rm str}$

Before we delve into the ILT analysis of the $M(t)$ data, let us first examine the consequence of the fit with the stretched exponential version of Eq. (4) commonly used in the

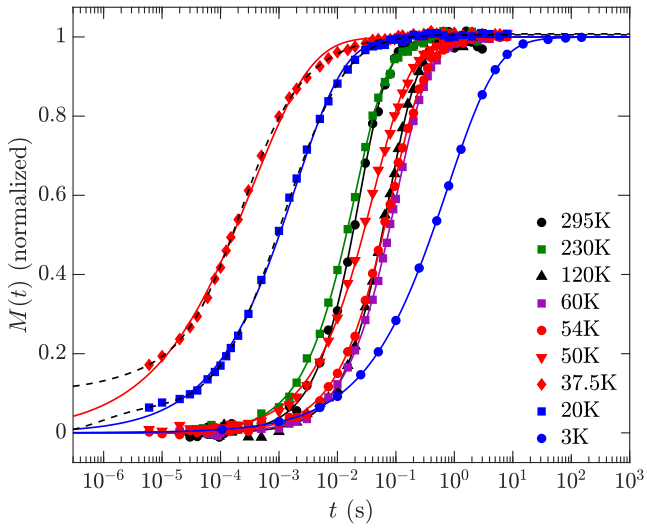

FIG. 2. ^{139}La NMR recovery curves $M(t)$ at representative temperatures, normalized by $(M(t) - M_0)/A + 1$, where M_0 and A are parameters from the best fits (solid curves) to the stretched exponential form in Eq. (7). Also shown are best fits to the ILT (dashed black lines) using Eq. (8) at 37.5 K and 20 K. Notice that the large distribution in $P(1/T_1)$ near $T_{\rm spin}^{\mu\rm SR}$ leads to poor stretched exponential fits at 37.5 K and 20 K, while the ILT yields good fits.

literature,

$$M(t) = M_0 - A\sum_{k=1}^{4} p_k e^{-\left(q_k t/T_1^{\rm str}\right)^{\beta}}, \qquad (7)$$

where the same normal modes k [29,30] are used as in Eq. (4) and $\sum_{k=1}^{4} p_k = 1$ is normalized. We caution that, unlike the case of $I = 1/2$, there is no mathematical justification to place the same β in all four terms, although we will show below that this phenomenological procedure works fairly well to estimate the log mean $1/T_1^{\rm lm}$ of the underlying probability density function $P(1/T_1)$.

We summarize $1/T_1^{\rm str}$ and β observed at the ^{139}La sites in Figs. 3(a) and 3(b), respectively. $1/T_1^{\rm str}$ begins to increase sharply at $T_{\rm charge}$, where charge order turns on a strong enhancement of low-frequency spin fluctuations in the charge-ordered domains [4,37]. Our finding is consistent with our powder NQR results by Hunt *et al.* [5] and a more recent single-crystal NMR report by Baek *et al.* [36]. $1/T_1^{\rm str}$ peaks around $T_{\rm spin}^{\mu\rm SR}$ and is progressively suppressed in the spin-ordered state.

Note that $1/T_1^{\rm str}$ is mildly enhanced near $T_{\rm HTT-LTO} \simeq 236$ K, where β shows a minimum. This is not due to enhanced spin fluctuations, but rather to the contribution of slow EFG fluctuations near the structural phase transitions. A proof may be found in ^{63}Cu NMR measurements of $1/T_1$, which show no anomalies at $T_{\rm HTT-LTO}$ [9,11,38]. $1/T_1$ is three orders of magnitude larger at the ^{63}Cu sites, owing to a much stronger hyperfine coupling with Cu electron spins and hence less sensitive to such slow EFG fluctuations near the structural phase transition [9,11,38]. Strictly speaking, one cannot rely on Eq. (4) or (7) under the presence of EFG contributions to the T_1 process. This is because Eq. (4) or (7) implicitly assume that only the magnetic transitions with $\Delta I_z = \pm 1$ between

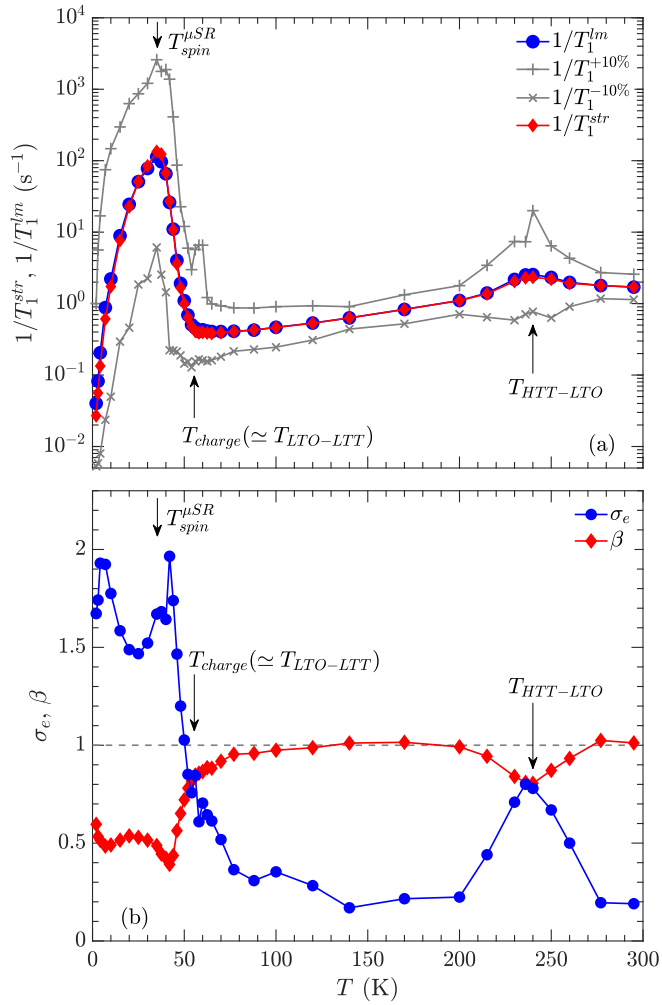

FIG. 3. (a) Temperature dependence of $1/T_1^{\rm str}$ (red symbols) obtained from the stretched fit with Eq. (7), and log-mean value $1/T_1^{\rm lm}$ (blue symbols) of the probability density $P(1/T_1)$ from Eq. (9), along with $1/T_1^{+10\%}$ ($1/T_1^{-10\%}$) at the top (bottom) 10% value of the distributed $P(1/T_1)$, respectively. $1/T_1^{\rm str}$ may be considered a close approximation to $1/T_1^{\rm lm}$. See Fig. 4 in Ref. [22] for the corresponding results observed for $La_{1.885}Sr_{0.115}CuO_4$. (b) Temperature dependence of the stretched exponent β, and standard deviation σ_e of $P(1/T_1)$ from Eq. (10). Note that σ_e and β are found to be anticorrelated [31].

two adjacent nuclear spin energy levels contribute to the T_1 process [29,30], whereas the EFG fluctuations induce $\Delta I_z = \pm 2$ transitions as well. In practice, it is difficult to determine the spin and EFG-induced $1/T_1$ contributions separately [39], and we phenomenologically rely on Eq. (7) to account for the enhanced $1/T_1$ due to the slowly fluctuating EFG.

Below $\simeq 200$ K down to $\simeq 80$ K, β is close to 1. This implies that the T_1 process is dominated by Cu spin fluctuations once the HTT-LTO structural phase transition is complete and the distribution of $1/T_1$ is small. In the case of the superconducting compositions above $x \simeq 1/8$, $1/T_1$ continues to decrease smoothly toward T_c [36,40,41]. In contrast, $1/T_1^{\rm str}$ in the present case begins to level off below $\simeq 80$ K, and β deviates from 1 again. In this temperature range, we expect a growth in nanoscale electronic inhomogeneity as we previously reported for $La_{2-x}Sr_xCuO_4$ [42].

In fact, we recently confirmed that $1/T_1$ at ^{63}Cu sites of the same $La_{1.875}Ba_{0.125}CuO_4$ crystal levels off below $\simeq 80$ K if measured with the pulse separation time $\tau = 2\,\mu$s between the 90- and 180-degree pulses, whereas $1/T_1$ keeps decreasing if measured with $\tau = 20\,\mu$s [38]. As such, our results below $\simeq 80$ K in Fig. 3 are consistent with enhanced spin fluctuations with growing spatial distributions. However, what about the potential influence of the dynamic short-range charge order observed above $T_{\rm charge}$ [8], and the slowing of phonons near the LTO to LTT transition toward $T_{\rm charge}$? The slowing fluctuations of charge and lattice would certainly induce slow EFG fluctuations that can potentially contribute to $1/T_1$, as observed near $T_{\rm HTT\text{-}LTO}$. We will address this issue below based on ILT in Sec. IV C.

B. The ILT results and consistency with the stretched fit

To account for the four normal modes for $I = 7/2$ in Eq. (4), we replaced Eq. (5) with the following:

$$M(t) = \sum_{j=1}^{m}\sum_{k=1}^{4}\left[1 - 2p_k e^{-q_k t/T_{1j}}\right]P(1/T_{1j}), \tag{8}$$

where the same normal modes k [29,30] are used as in Eq. (4) and $\sum_{k=1}^{4} p_k = 1$ is normalized. The summation $\sum_{j=1}^{m} P(1/T_{1j}) = M_0$ is the saturated value of the magnetization and $m = 250$ is the chosen number of logarithmically spaced bins ranging from $10^{-3}\,\mathrm{s}^{-1} \leqslant 1/T_{1j} \leqslant 10^{5}\,\mathrm{s}^{-1}$. The probability density is then normalized to $\sum_{j=1}^{m} P(1/T_{1j})\,\Delta_P = 1$, where the constant $\Delta_P = \log_{10}(1/T_{1j+1}) - \log_{10}(1/T_{1j}) = 0.0321$ is the logarithmic bin spacing. This normalization ensures a 1–1 comparison of $P(1/T_1)$'s when the bin spacing is different for each $P(1/T_1)$. Using a $\log_{10}$ base to define Δ_P conveniently yields unit area for a square $P(1/T_1)$ distribution a decade wide and of unit height.

In Fig. 4, we summarize the ILT curves $P(1/T_1)$ obtained from $M(t)$ at representative temperatures. We also show the evolution of $P(1/T_1)$ with temperature in the color contour map in Fig. 5. From each of these ILT curves, we deduced $1/T_1^{\rm lm}$ and σ_e, the log mean of the distribution $P(1/T_1)$ and the log-standard deviation of $1/T_1$, respectively, as such,

$$\ln(1/T_1^{\rm lm}) = \sum_{j=1}^{m} \ln(1/T_{1j})P(1/T_{1j})\Delta_P, \tag{9}$$

$$\sigma_e^2 = \sum_{j=1}^{m}\left[\ln(1/T_{1j}) - \ln\left(1/T_1^{\rm lm}\right)\right]^2 P(1/T_{1j})\Delta_P, \tag{10}$$

where $\sum_{j=1}^{m} P(1/T_{1j})\,\Delta_P = 1$. We use the subscript e in σ_e to emphasize that the logarithm to base e (i.e., the natural logarithm) is used to compute the log-standard deviation. We summarize $1/T_1^{\rm lm}$ in comparison to $1/T_1^{\rm str}$ in Fig. 3(a), while σ_e is compared with β in Fig. 3(b). $1/T_1^{\rm str}$ and $1/T_1^{\rm lm}$ agree well. That is, $1/T_1^{\rm str}$ estimated from the phenomenological stretch fit may be considered as a good approximation for the average value of the distributed $1/T_1$. σ_e also shows clear anticorrelation with β. This also makes sense. β becomes smaller than 1 when $1/T_1$ develops a distribution, whereas σ_e increases when the distribution of $1/T_1$ grows and $P(1/T_1)$ becomes wider. Thus we have established that our ILT results encompass the equivalent information as the stretched exponential analysis of $M(t)$. Note, however, that besides $1/T_1^{\rm str}$ and β, the stretched exponential analysis loses all other information about the underlying probability density $P(1/T_1)$. In the Supplemental Material [31], we present details of the ILT analysis, including the concept of "resolution" and uncertainties in $P(1/T_1)$.

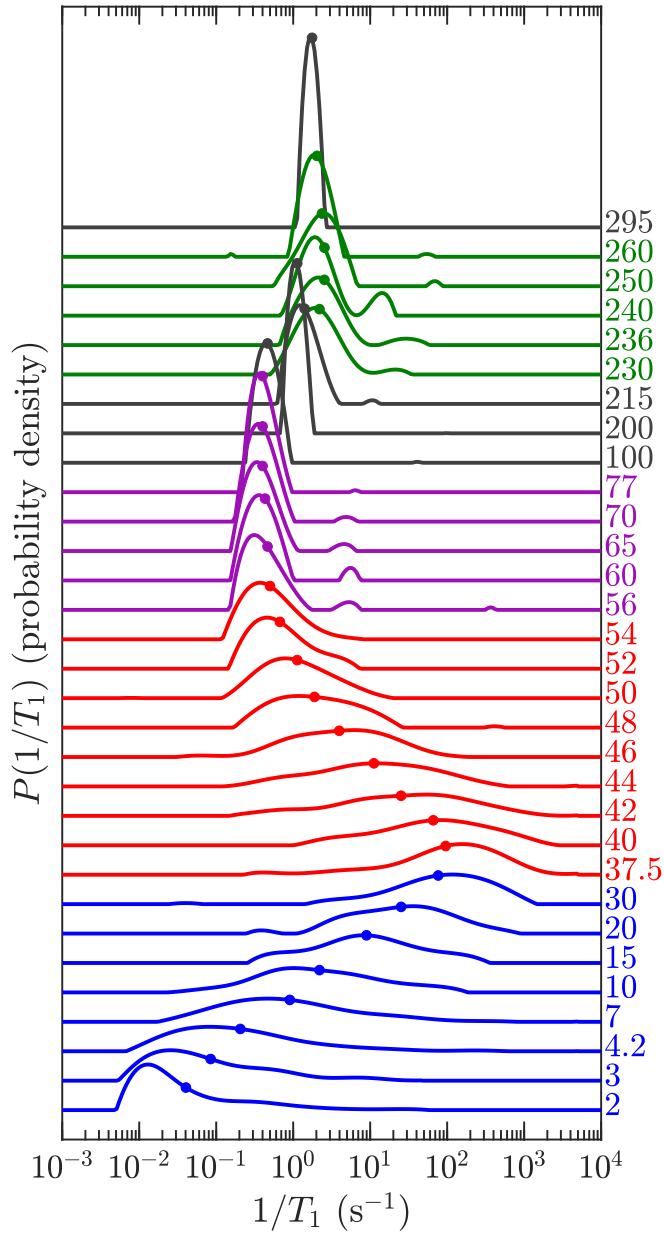

FIG. 4. Representative results of $P(1/T_1)$ (probability density) obtained from $M(t)$ based on ILT. For clarity, the origin of the vertical axes are shifted at each temperature, where the temperature T(K) is listed on the right-hand side. The location of the log means $1/T_1^{\rm lm}$ (•) are shown on each $P(1/T_1)$.

C. Distribution of $1/T_1$

Having established the validity of the ILT, let us take an additional step and look into exactly how the distribution of $1/T_1$ develops. At the top of Fig. 4 is the $P(1/T_1)$ result at 295 K shown in dark gray. $P(1/T_1)$ is single peaked, with

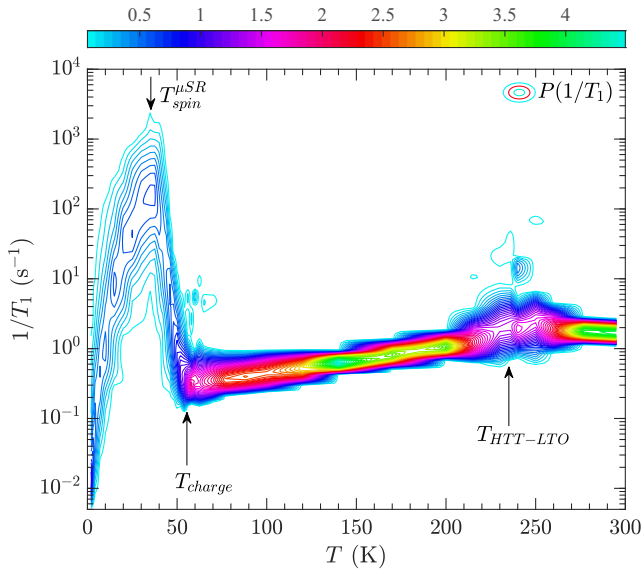

FIG. 5. Contour map of $P(1/T_1)$ (probability density) generated from ILT, using 64 contours. Color bar scale is shown at the top of the figure.

the log mean at $1/T_1^{\rm lm} = 1.7\,{\rm s}^{-1}$. Note that the stretched exponential fit of $M(t)$ returns $\beta = 1.01$ at 295 K, and hence the distribution of $1/T_1$ is minimal. The finite width of $P(1/T_1)$ at 295 K primarily originates from the finite signal-to-noise ratio of the measurement [31].

We summarize the $P(1/T_1)$ curves in the vicinity of $T_{\rm HTT\text{-}LTO} \simeq 235$ K in green in Fig. 4. Two noticeable changes take place near $T_{\rm HTT\text{-}LTO}$. First, the main peak of $P(1/T_1)$ shifts to the right, accompanied by significant broadening. The small shift corresponds to the small increase observed for $1/T_1^{\rm lm}$ as well as $1/T_1^{\rm str}$. The broadening is a consequence of the additional transitions caused by EFG fluctuations, which are not explicitly taken into account in Eq. (8). Second, a small but noticeable split-off peak consistently emerges with $1/T_1 \simeq 20\,{\rm s}^{-1}$. Note that this does not necessarily mean that the EFG-induced transition has an order of magnitude faster $1/T_1$ in a small volume fraction of the sample. As noted above, the additional contributions by the fluctuating EFG to the relaxation processes with $\Delta I_z = \pm 1$ and ± 2 could significantly modify the relaxation function itself; we take this effect into account only phenomenologically in Eq. (8) which is derived for purely magnetic relaxation. The slow EFG fluctuations cease to exist when the second-order structural phase transition is complete, and the split-off peak disappears as we go deeper into the LTO structure below $T_{\rm HTT\text{-}LTO}$. $P(1/T_1)$ regains a narrower, single-peaked structure at 215 K and below down to 100 K, as shown by dark gray curves.

The ILT results from $\simeq 80$ K down to $T_{\rm charge} \simeq 54$ K are shown in purple. We recall that the charge-order transition is accompanied by a nearly first-order LTO to LTT structural phase transition [6,8]. Interestingly, a split-off peak analogous to that observed around $T_{\rm HTT\text{-}LTO}$ emerges again, signaling the presence of slow EFG fluctuations at the NMR frequency scale. In a separate study based on ^{63}Cu NMR, we show that the ^{63}Cu NMR line shape exhibits strong magnetic broadening in this temperature range below $\simeq 80$ K prior to the onset of long-range charge order at $T_{\rm charge}$. Moreover, ^{63}Cu $1/T_1$ begins to distribute [38]. Taken together, these findings suggest that, regardless of the exact origin of the slow EFG fluctuations above $T_{\rm charge}$ detected here, spin correlations grow hand in hand with the slow lattice and/or charge fluctuations below $\simeq 80$ K.

We use red curves to show the ILT results in the charge-ordered state below $T_{\rm charge} \simeq 54$ K down to the spin-ordering temperature $T_{\rm spin}^{\mu\rm SR} \simeq 35$ K. At 54 K, the split-off peak due to EFG fluctuations is suppressed. This is consistent with the nearly first-order nature of the simultaneous LTT and charge-order transitions [6,8]. Once entering the long-range charge-ordered state, $P(1/T_1)$ begins to broaden asymmetrically by transferring some spectral weight to larger values of $1/T_1$. At 48 K, approximately 1/3 of the spectral weight still remains at $1/T_1 \simeq 1\,{\rm s}^{-1}$ or below, although the fastest component reaches $1/T_1 \simeq 30\,{\rm s}^{-1}$. In other words, not all the Cu spin fluctuations begin to slow down and enhance $1/T_1$ immediately below $T_{\rm charge}$. Upon further cooling, the entire $P(1/T_1)$ curve shifts to larger values of $1/T_1$ while increasing in width. All ^{139}La nuclear spins relax with highly enhanced $1/T_1$ by 37 K, followed by spin ordering at $T_{\rm spin}^{\mu\rm SR} \simeq 35$ K. A physical picture that emerges from these observations is that *the volume fraction of the canonically behaving segments of* CuO_2 *planes with slow* $1/T_1$ *values gradually decreases below* $T_{\rm charge}$, and the spin order at the relatively slow measurement timescale of μSR experiments sets in when $\sim$100% volume fraction of the CuO_2 planes is under the influence of enhanced spin fluctuations triggered by charge order.

We summarize the ILT results below $T_{\rm spin}^{\mu\rm SR}$ using blue curves. The ILT curve $P(1/T_1)$ progressively shifts its weight to lower values of $1/T_1$ as the fluctuating spins freeze toward the base temperature. By 7 K, a majority of ^{139}La sites relax with $1/T_1 \simeq 1\,{\rm s}^{-1}$ or slower. It is in this temperature range where Zeeman-perturbed ^{63}Cu NQR signals become observable with increasing intensity [5,10], since the hyperfine magnetic field from frozen Cu moments become static at the NMR measurement timescale. In a separate work, we will demonstrate that a cutoff introduced for $P(1/T_1)$ can naturally account for the fraction of the observable ^{63}Cu NMR signal intensity that arises from canonically behaving domains below $T_{\rm charge}$, i.e., ^{63}Cu signal intensity wipeout effects [38].

D. Comparison with $La_{1.885}Sr_{0.115}CuO_4$

In Fig. 6, we compare the $P(1/T_1)$ results for $La_{1.875}Ba_{0.125}CuO_4$ with our earlier report for $La_{1.885}Sr_{0.115}CuO_4$ [22]. $P(1/T_1)$ for $La_{1.885}Sr_{0.115}CuO_4$ begins to broaden below the onset of its charge order at $T_{\rm charge} \simeq 80$ K [43–45], without exhibiting the split-off peak arising from EFG fluctuations. Since no LTT structural phase transition exists in $La_{1.885}Sr_{0.115}CuO_4$, this might be an indication that the signature of the EFG fluctuations observed above $T_{\rm charge}$ in the present case of $La_{1.875}Ba_{0.125}CuO_4$ is due primarily to the slow lattice fluctuations rather than slow charge fluctuations. On the other hand, the Bragg peaks associated with charge order in $La_{1.885}Sr_{0.115}CuO_4$ are known to be very weak and hence charge fluctuations may also be too weak to induce the split-off peak in $P(1/T_1)$.

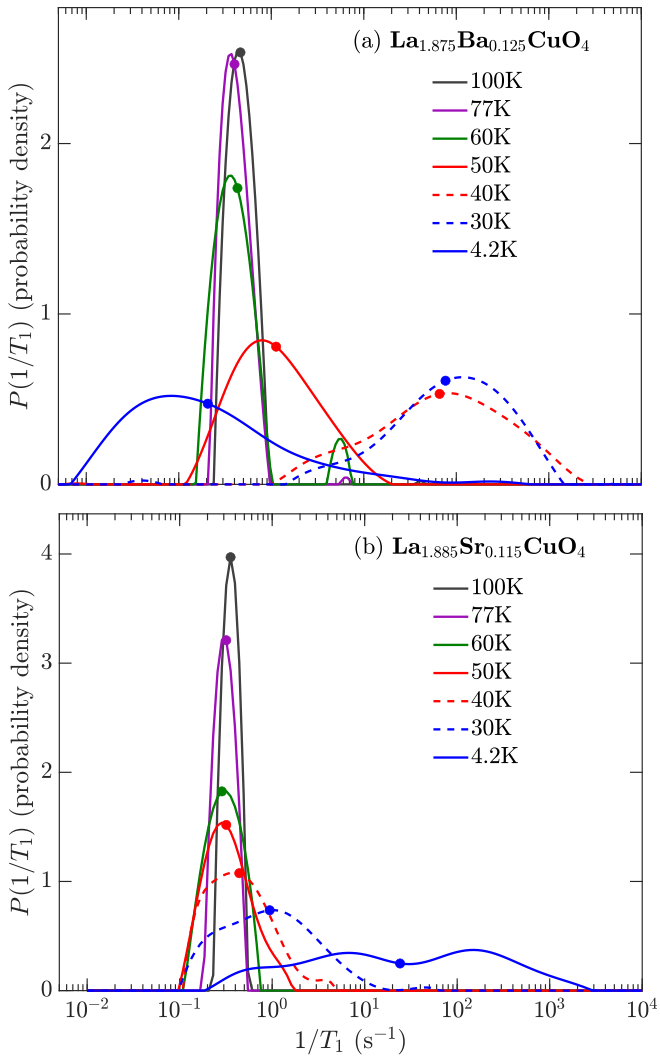

FIG. 6. Comparison of the $P(1/T_1)$ (probability density) between (a) $La_{1.875}Ba_{0.125}CuO_4$ (this paper, $T_{charge} \simeq 54$ K, $T_c = 4$ K) and, (b) $La_{1.885}Sr_{0.115}CuO_4$ (adopted from Ref. [46], $T_{charge} \simeq 80$ K, $T_c = 31$ K), at selected temperatures. The location of the log means $1/T_1^{lm}$ (•) are shown on each $P(1/T_1)$.

Another interesting aspect is the qualitative difference in the way the distribution of $P(1/T_1)$ develops. In the case of $La_{1.885}Sr_{0.115}CuO_4$, notice that $P(1/T_1)$ continues to transfer its spectral weight to smaller values down to $1/T_1 \simeq 0.1\,s^{-1}$ even below $T_{charge} \simeq 80$ K, although the log mean of the distribution is shifting to larger values of $1/T_1$. This means that $1/T_1$ continues to become smaller at a substantial fraction of ^{139}La sites even deep inside the charge-ordered state below $T_{charge} \simeq 80$ K. The temperature dependence of $1/T_1$ at these ^{139}La sites is qualitatively the same as that in the canonical superconducting CuO_2 planes in $La_{1.85}Sr_{0.15}CuO_4$ [36,40,41]. It is just that the *volume fraction* of such canonically superconducting domains gradually decreases below T_{charge}. As a consequence, we can clearly see that the peak structure from the canonically behaving domains is still visible as a clearly identifiable shoulder at $1/T_1 \simeq 0.1\,s^{-1}$ down to ~30 K. This conclusion was corroborated by the fact that two types of ^{63}Cu NMR signals exist in $La_{1.885}Sr_{0.115}CuO_4$, too: The winglike signal is extremely broad and with large $1/T_1$, whereas the canonically behaving signal has a narrow line shape with slow $1/T_1$ that is comparable to the optimally doped superconductor with $x = 0.15$ [47].

In contrast, the slow shoulder at $1/T_1 \simeq 0.1\,s^{-1}$ observed for $La_{1.885}Sr_{0.115}CuO_4$ is not observable in the present case of $La_{1.875}Ba_{0.125}CuO_4$. As temperature decreases below $T_{charge} \simeq 54$ K, $P(1/T_1)$ shifts to larger values of $1/T_1$ more quickly. There is only a hint of a slow shoulder at $1/T_1 \simeq 3\,s^{-1}$ from 54 K down to 48 K in Fig. 4. We confirmed that the ^{63}Cu NMR line shape for $La_{1.875}Ba_{0.125}CuO_4$ broadens more homogeneously below $\simeq 80$ K, and lacks the aforementioned two-component wing plus narrow-peak structure observed for $La_{1.885}Sr_{0.115}CuO_4$ [38]. In short, CuO_2 planes in $La_{1.875}Ba_{0.125}CuO_4$ are more homogeneously affected by charge order and accompanying enhancements of slow spin fluctuations, which increases $1/T_1$.

V. SUMMARY AND CONCLUSIONS

We have reported the ILTT$_1$ analysis to demonstrate how the distribution of $1/T_1$ develops in charge-ordered $La_{1.875}Ba_{0.125}CuO_4$. We identified the signature of the slow EFG fluctuations near $T_{HTT\text{-}LTO}$ and showed that the same signature reemerges above T_{charge}. Our experiments and ILTT$_1$ analysis cannot determine whether the source of the slow EFG fluctuations is the lattice and/or charge vibrations.

By comparing the probability density function $P(1/T_1)$ from ILTT$_1$ analysis, we demonstrated that the magnetic properties of the CuO_2 planes become highly inhomogeneous below $T_{charge} \simeq 54$ K, and domains with canonical behavior of a high T_c superconductor persist even below T_{charge}. These residual domains are oblivious to the charge-order transition, and spin fluctuations are not anomalously enhanced. This suggests that charge order does not set in homogeneously at T_{charge} in the entire CuO_2 planes. This finding is consistent with the fact that the width of the charge-order Bragg peaks (i.e., the inverse of the charge order correlation length) is not resolution limited above $\simeq 40$ K, and hence the size of the charge-ordered domains is not infinite [8].

The volume fraction of these residual domains gradually diminishes below $T_{charge} \simeq 54$ K in $La_{1.875}Ba_{0.125}CuO_4$. By 40 K, nearly $\simeq 100\%$ volume of the CuO_2 planes have large $1/T_1$ induced by enhanced low-frequency Cu spin fluctuations triggered by charge order. This finding is in stark contrast with the case of $La_{1.885}Sr_{0.115}CuO_4$, where a significant fraction of domains in the CuO_2 planes still exhibits characteristic behavior of high T_c superconductor with slowing $1/T_1$ at 40 K [22,46]. These contrasting behaviors are consistent with the fact that superconductivity sets in at as high as $T_c = 31$ K for $La_{1.885}Sr_{0.115}CuO_4$, while superconductivity is strongly suppressed to $T_c = 4$ K in $La_{1.875}Ba_{0.125}CuO_4$.

The present paper also highlights the usefulness of the ILTT$_1$ analysis technique in general. The ILT provides us with much richer information than the conventional stretched fit analysis since ILT generates the probability density function $P(1/T_1)$ rather than just the average value of $1/T_1$. Moreover, it is important to note that ILTT$_1$ analysis is unbiased, and one does not need to assume the shape of the distribution function $P(1/T_1)$. The ILTT$_1$ analysis, which has been used

successfully in NMR petrophysics, has the potential to revolutionize NMR research of quantum materials with disorder.

Finally, we briefly comment on some earlier publications, in which several groups tried to model the distribution of $1/T_1$ in cuprates [5,48,49] and unrelated materials [50,51]. Note that all these earlier attempts were made by assuming a functional form of $P(1/T_1)$ upfront, which may or may not reflect the reality. For example, our earlier attempt in 2001 assumed a symmetrical Gaussian distribution of $1/T_1$ on a log scale in the charge-ordered state of cuprates for fitting $M(t)$, as shown in Fig. 12 of Ref. [5]. The present paper shows that such a symmetrical functional form is only approximately true for $La_{1.875}Ba_{0.125}CuO_4$ in a limited temperature range and invalid for $La_{1.885}Sr_{0.115}CuO_4$ [22]. Reference [48] assumed instead that magnetic inhomogeneity of the CuO_2 planes in Eu codoped 214 cuprates is caused entirely by preexisting quenched disorder, which gives rise to a Gaussian distribution in an activation energy for spin fluctuations rather than the distribution of $1/T_1$ itself. Since their toy model is based on an incorrect assumption that charge-order transition does not exist, all the NMR properties are expected to evolve smoothly, in contradiction with the experimental reality such as Fig. 3(a). Reference [49] extended our earlier analysis in Ref. [5], and assumed a symmetrical distribution function for $1/T_1$ on a log scale for $La_{1.88}Sr_{0.12}CuO_4$ [49]. Despite the unrealistic assumption in contradiction to the experimental reality of nonsymmetric $P(1/T_1)$ [22], their analysis actually showed the onset of unusual NMR anomalies starting from $\simeq 80$ K. However, the authors in Ref. [49] did not attribute their findings to the onset of charge order, as they had been advocating for the absence of charge order in the superconducting phase of $La_{2-x}Sr_xCuO_4$.

ACKNOWLEDGMENTS

The authors thank J. Wang for helpful discussions. P.M.S. is supported by The Rice University Consortium for Processes in Porous Media. The work at McMaster is supported by NSERC. The work at Tohoku is supported by Grant-in-Aid for Scientific Research (A) (16H02125), Japan.

[1] J. D. Axe, A. H. Moudden, D. Hohlwein, D. E. Cox, K. M. Mohanty, A. R. Moodenbaugh, and Y. Xu, Structural Phase Transformations and Superconductivity in $La_{2-x}Ba_xCuO_4$, Phys. Rev. Lett. **62**, 2751 (1989).

[2] G. M. Luke, L. P. Le, B. J. Strenlieb, W. D. Wu, Y. J. Uemura, J. H. Brewer, T. M. Riseman, S. Ishibashi, and S. Uchida, Static magnetic order in $La_{1.875}Ba_{0.125}CuO_4$, Physica C **185–189**, 1175 (1991).

[3] J. M. Tranquada, B. J. Sternlieb, J. D. Axe, Y. Nakamura, and S. Uchida, Evidence for stripe correlations in copper oxide superconductors, Nature **375**, 561 (1995).

[4] A. W. Hunt, P. M. Singer, K. R. Thurber, and T. Imai, ^{63}Cu NQR Measurement of Stripe Order Parameter in $La_{2-x}Sr_xCuO_4$, Phys. Rev. Lett. **82**, 4300 (1999).

[5] A. W. Hunt, P. M. Singer, A. F. Cederström, and T. Imai, Glassy slowing of stripe modulation in $(La, Eu, Nd)_{2-x}(Sr, Ba)_xCuO_4$: A ^{63}Cu and ^{139}La NQR study down to 350 mK, Phys. Rev. B **64**, 134525 (2001).

[6] M. Fujita, H. Goka, K. Yamada, J. M. Tranquada, and L. P. Regnault, Stripe order, depinning, and fluctuations in $La_{1.875}Ba_{0.125}CuO_4$ and $La_{1.875}Ba_{0.075}Sr_{0.050}CuO_4$, Phys. Rev. B **70**, 104517 (2004).

[7] V. Thampy, X. M. Chen, Y. Cao, C. Mazzoli, A. M. Barbour, W. Hu, H. Miao, G. Fabbris, R. D. Zhong, G. D. Gu, J. M. Tranquada, I. K. Robinson, S. B. Wilkins, and M. P. M. Dean, Static charge-density-wave order in the superconducting state of $La_{2-x}Ba_xCuO_4$, Phys. Rev. B **95**, 241111(R) (2017).

[8] H. Miao, R. Fumagalli, M. Rossi, J. Lorenzana, G. Seibold, F. Yakhou-Harris, K. Kummer, N. B. Brookes, G. D. Gu, L. Braicovich, G. Ghiringhelli, and M. P. M. Dean, Formation of Incommensurate Charge Density Waves in Cuprates, Phys. Rev. X **9**, 031042 (2019).

[9] T. Imai, K. Yoshimura, T. Uemura, H. Yasuoka, and K. Kosuge, ^{63}Cu NMR study of spin dynamics in $La_{2-x}(Sr, Ba)_xCuO_y$ $(0.04 \leqslant x \leqslant 0.16,\ 3.99 \leqslant y \leqslant 4.03)$, J. Phys. Soc. Jpn. **59**, 3846 (1990).

[10] H. Tou, M. Matsumura, and H. Yamagata, Anomalous Cu-NQR spectral change due to low-temperature structural transition around $x = 0.06$ in $(La_{1-x}Ba_x)_2CuO_4$, J. Phys. Soc. Jpn. **61**, 1477 (1992).

[11] H. Tou, M. Matsumura, and H. Yamagata, ^{63}Cu nuclear spin-lattice relaxation study for low-temperature structural transition in $(La_{1-x}Ba_x)_2CuO_4$ around $x = 0.06$, J. Phys. Soc. Jpn. **62**, 1474 (1993).

[12] K. Kumagai, K. Kawano, I. Watanabe, K. Nishiyama, and K. Nagamine, μSR and NMR investigations on electronic and magnetic state around $x = 0.12$ in $La_{2-x}Sr_xCuO_4$ and $La_{2-x}Ba_xCuO_4$, Hyperfine Interact. **86**, 473 (1994).

[13] T. Goto, S. Kazama, K. Miyagawa, and T. Fukase, $^{63/65}$Cu/^{139}La-NMR study on antiferromagnetic ordering in high-T_c oxides $La_{2-x}Sr_xCuO_4$ ($x \simeq 0.115$) and $La_{2-x}Ba_xCuO_4$ ($x \simeq 0.125$), J. Phys. Soc. Jpn. **63**, 3494 (1994).

[14] S.-H. Baek, Y. Utz, M. Hücker, G. D. Gu, B. Büchner, and H.-J. Grafe, Magnetic field induced anisotropy of ^{139}La spin-lattice relaxation rates in stripe ordered $La_{1.875}Ba_{0.125}CuO_4$, Phys. Rev. B **92**, 155144 (2015).

[15] D. Pelc, H.-J. Grafe, G. D. Gu, and M. Požek, Cu nuclear magnetic resonance study of charge and spin stripe order in $La_{1.875}Ba_{0.125}CuO_4$, Phys. Rev. B **95**, 054508 (2017).

[16] D. C. Johnston, S.-H. Baek, X. Zong, F. Borsa, J. Schmalian, and S. Kondo, Dynamics of Magnetic Defects in Heavy Fermion LiV_2O_4 from Stretched Exponential ^{7}Li NMR Relaxation, Phys. Rev. Lett. **95**, 176408 (2005).

[17] L. Venkataramanan, Y.-Q. Song, and M. D. Hürlimann, Solving Fredholm integrals of the first kind with tensor product structure in 2 and 2.5 dimensions, IEEE Trans. Sig. Process. **50**, 1017 (2002).

[18] Y.-Q. Song, L. Venkataramanan, M. D. Hürlimann, M. Flaum, P. Frulla, and C. Straley, T_1-T_2 correlation spectra obtained using fast two-dimensional laplace inversion, J. Magn. Reson. **154**, 261 (2002).

[19] J. Mitchell, T. C. Chandrasekera, and L. Gladden, Numerical estimation of relaxation and diffusion distributions in two dimensions, Prog. Nucl. Magn. Reson. Spectrosc. **62**, 34 (2012).

[20] P. M. Singer, D. Asthagiri, Z. Chen, A. Valiya Parambathu, G. J. Hirasaki, and W. G. Chapman, Role of internal motions and molecular geometry on the NMR relaxation of hydrocarbons, J. Chem. Phys. **148**, 164507 (2018).

[21] P. M. Singer, D. Asthagiri, W. G. Chapman, and G. J. Hirasaki, NMR spin-rotation relaxation and diffusion of methane, J. Chem. Phys. **148**, 204504 (2018).

[22] A. Arsenault, T. Imai, P. M. Singer, K. M. Suzuki, and M. Fujita, Magnetic inhomogeneity in charge-ordered $La_{1.885}Sr_{0.115}CuO_4$ studied by NMR, Phys. Rev. B **101**, 184505 (2020).

[23] S. K. Takahashi, J. Wang, A. Arsenault, T. Imai, M. Abramchuk, F. Tafti, and P. M. Singer, Spin Excitations of a Proximate Kitaev Quantum Spin Liquid Realized in Cu_2IrO_3, Phys. Rev. X **9**, 031047 (2019).

[24] M. Itoh, H. Yasuoka, A. R. King, and V. Jaccarino, Decay of the nuclear magnetization in the randomly diluted antiferromagnets $Fe_xZn_{1-x}F_2$ and $Mn_xZn_{1-x}F_2$, J. Phys. Soc. Jpn. **55**, 964 (1986).

[25] P. Thayamballi and D. Hone, Nuclear relaxation in a randomly diluted Heisenberg paramagnet, Phys. Rev. B **21**, 1766 (1980).

[26] T. Imai, T. Shimizu, T. Tsuda, H. Yasuoka, T. Takabatake, Y. Nakazawa, and M. Ishikawa, Nuclear spin-lattice relaxation of ^{63,65}Cu at the Cu(2) sites of the high T_c superconductor $YBa_2Cu_3O_{7-\delta}$, J. Phys. Soc. Jpn. **57**, 1771 (1988).

[27] T. Imai, T. Shimizu, H. Yasuoka, Y. Ueda, and K. Kosuge, Anomalous temperature dependence of Cu nuclear spin-lattice relaxation in $YBa_2Cu_3O_{6.91}$, J. Phys. Soc. Jpn. **57**, 2280 (1988).

[28] T. Imai, H. Yasuoka, T. Shimizu, Y. Ueda, K. Yoshimura, and K. Kosuge, Cu spin dyanmics in high T_c and related oxides investigated by nuclear spin-lattice relaxation, Physica C **162–164**, 169 (1989).

[29] E. R. Andrew and D. P. Tunstall, Spin-lattice relaxation in imperfect cubic crystals and in non-cubic crystals, Proc. R. Soc. **78**, 1 (1961).

[30] A. Narath, Nuclear spin-lattice relaxation in hexagonal transition metals: Titanium, Phys. Rev. **162**, 320 (1967).

[31] See Supplemental Material at http://link.aps.org/supplemental/10.1103/PhysRevB.101.174508 for technical details of ILT.

[32] E. Chouzenoux, S. Moussaoui, J. Idier, and F. Mariette, Efficient maximum entropy reconstruction of nuclear magnetic resonance T_1-T_2 spectra, IEEE Trans. Sig. Process. **58**, 6040 (2010).

[33] M. Prange and Y.-Q. Song, Quantifying uncertainty in NMR T_2 spectra using Monte Carlo inversion, J. Magn. Reson. **196**, 54 (2009).

[34] L. Venkataramanan, F. K. Gruber, T. M. Habashy, and D. E. Freed, Mellin transform of CPMG data, J. Magn. Reson. **206**, 20 (2010).

[35] E. J. Fordham, L. Venkataramanan, J. Mitchell, and A. Valori, What are, and what are not inverse Laplace transforms, Diffusion Fundam. **29**, 2 (2017).

[36] S.-H. Baek, A. Erb, and B. Büchner, Low-energy spin dynamics and critical hole concentrations in $La_{2-x}Sr_xCuO_4$ ($0.07 \leqslant x \leqslant 0.2$) revealed by ^{139}La and ^{63}Cu nuclear magnetic resonance, Phys. Rev. B **96**, 094519 (2017).

[37] J. M. Tranquada, N. Ichikawa, and S. Uchida, Glassy nature of stripe ordering in $La_{1.6-x}Nd_{0.4}Sr_xCuO_4$, Phys. Rev. B **59**, 14712 (1999).

[38] T. Imai, A. Arsenault, P. M. Singer, and M. Fujita, Revisitng ^{63}Cu NMR evidence for charge order in $La_{1.875}Ba_{0.125}CuO_4$ (unpublished).

[39] A. Suter, M. Mali, J. Roos, and D. Brinkmann, Mixed magnetic and quadrupolar relaxation in the presence of a dominant static Zeeman Hamiltonian, J. Phys.: Condens. Matter **10**, 5977 (1998).

[40] T. Kobayashi, S. Wada, Y. Kitaoka, and K. Asayama, Nuclear spin-lattice relaxation of ^{139}La in superconducting $(La_{1-x}Sr_x)_2CuO_4$, J. Phys. Soc. Jpn. **58**, 2662 (1989).

[41] K. Yoshimura, T. Uemura, M. Kato, T. Shibata, K. Kosuge, T. Imai, and H. Yasuoka, Magnetic phase differentiation in the $La_{2-x}Sr_xCuO_y$ systems—Cu and La nuclear quadrupole resonance and relaxation, Springer Proc. Phys. **60**, 405 (1992).

[42] P. M. Singer, A. W. Hunt, and T. Imai, ^{63}Cu NQR Evidence for Spatial Variation of Hole Concentration in $La_{2-x}Sr_xCuO_4$, Phys. Rev. Lett. **88**, 047602 (2002).

[43] T. P. Croft, C. Lester, M. S. Senn, A. Bombardi, and S. M. Hayden, Charge density wave fluctuations in $La_{2-x}Sr_xCuO_4$ and their competition with superconductivity, Phys. Rev. B **89**, 224513 (2014).

[44] V. Thampy, M. P. M. Dean, N. B. Christensen, L. Steinke, Z. Islam, M. Oda, M. Ido, N. Momono, S. B. Wilkins, and J. P. Hill, Rotated stripe order and its competition with superconductivity in $La_{1.88}Sr_{0.12}CuO_4$, Phys. Rev. B **90**, 100510(R) (2014).

[45] J. Wen, H. Huang, S. J. Lee, H. Jang, J. Knight, Y. S. Lee, M. Fujita, K. M. Suzuki, S. Asano, S. A. Kivelson, C. C. Kao, and J.-S. Lee, Observation of two types of charge-density wave orders in superconducting $La_{2-x}Sr_xCuO_4$, Nat. Commun. **10**, 3269 (2019).

[46] A. Arsenault, S. K. Takahashi, T. Imai, W. He, Y. S. Lee, and M. Fujita, ^{139}La NMR investigation of the charge and spin order in a $La_{1.885}Sr_{0.115}CuO_4$ single crystal, Phys. Rev. B **97**, 064511 (2018).

[47] T. Imai, S. K. Takahashi, A. Arsenault, A. W. Acton, D. Lee, W. He, Y. S. Lee, and M. Fujita, Revisiting ^{63}Cu NMR evidence for charge order in superconducting $La_{1.885}Sr_{0.115}CuO_4$, Phys. Rev. B **96**, 224508 (2017).

[48] N. J. Curro, P. C. Hammel, B. J. Suh, M. Hücker, B. Büchner, U. Ammerahl, and A. Revcolevschi, Inhomogeneous Low Frequency Spin Dynamics in $La_{1.65}Eu_{0.2}Sr_{0.15}CuO_4$, Phys. Rev. Lett. **85**, 642 (2000).

[49] V. F. Mitrović, M.-H. Julien, C. de Vaulx, M. Horvatić, C. Berthier, T. Suzuki, and K. Yamada, Similar glassy features in the ^{139}La NMR response of pure and disordered $La_{1.88}Sr_{0.12}CuO_4$, Phys. Rev. B **78**, 014504 (2008).

[50] J. Gezo, T.-K. Lui, B. Wolin, C. P. Slichter, R. Giannetta, and J. A. Schlueter, Stretched exponential spin relaxation in organic superconductors, Phys. Rev. B **88**, 140504(R) (2013).

[51] A. P. Dioguardi, M. M. Lawson, B. T. Bush, J. Crocker, K. R. Shirer, D. M. Nisson, T. Kissikov, S. Ran, S. L. Bud'ko, P. C. Canfield, S. Yuan, P. L. Kuhns, A. P. Reyes, H.-J. Grafe, and N. J. Curro, NMR evidence for inhomogeneous glassy behavior driven by nematic fluctuations in iron arsenide superconductors, Phys. Rev. B **92**, 165116 (2015).